



Politecnico  
di Bari

Repository Istituzionale dei Prodotti della Ricerca del Politecnico di Bari

Numerical study of the effect of freestream turbulence on by-pass transition in a boundary layer

This is a post print of the following article

*Original Citation:*

Numerical study of the effect of freestream turbulence on by-pass transition in a boundary layer / Cherubini, S., Robinet, J.C., DE PALMA, P.. - In: ENERGY PROCEDIA. - ISSN 1876-6102. - 45:(2014), pp. 578-587.  
[10.1016/j.egypro.2014.01.062]

*Availability:*

This version is available at <http://hdl.handle.net/11589/3591> since: 2016-01-09

*Published version*

DOI:10.1016/j.egypro.2014.01.062

Publisher:

*Terms of use:*

(Article begins on next page)

68th Conference of the Italian Thermal Machines Engineering Association, ATI2013

## Numerical study of the effect of freestream turbulence on by-pass transition in a boundary layer

Stefania Cherubini<sup>a</sup>, Jean-Christophe Robinet<sup>a</sup>, Pietro De Palma<sup>b,\*</sup>

<sup>a</sup>*DynFluid, Arts et Métiers ParisTech, 151, Bd. de l'Hopital, 75013 Paris, France*

<sup>b</sup>*DIMMM and CEMeC, Politecnico di Bari, via Re David 200, 70125 Bari, Italy*

### Abstract

We use direct numerical simulations in the presence of free-stream turbulence having different values of intensity,  $Tu$ , and integral length scale,  $L$ , in order to determine which kind of structures are involved in the path to transition of a boundary-layer flow. The main aim is to determine under which conditions the path to transition involves structures similar to the linear or non-linear optimal perturbations. For high values of  $Tu$  and  $L$ , we observe a large-amplitude path to transition characterized by localized vortical structures and patches of high- and low-momentum fluctuations. Such a scenario is found to correlate well with the  $\Lambda$  and hairpin structures resulting from the time evolution of non-linear optimal perturbations, whereas, for lower  $Tu$  and  $L$ , a larger correlation is found with respect to linear optimal disturbances. This indicates that a large-amplitude path to transition exists, different from the one characterized by elongated streaks undergoing secondary instability. To distinguish between the two transition scenarios, a simple parameter linked to the streamwise localisation of high- and low-momentum zones is introduced. Finally, an accurate law to predict the transition location is provided, taking into account both  $Tu$  and  $L$ , valid for both the transition scenarios.

© 2013 The Authors. Published by Elsevier Ltd. Open access under [CC BY-NC-ND license](https://creativecommons.org/licenses/by-nc-nd/4.0/).

Selection and peer-review under responsibility of ATI NAZIONALE

*Keywords:* Transition to turbulence; boundary-layer flows; optimal perturbations.

### 1. Introduction

Transition from laminar to turbulent flow has a relevant role in many energy-production devices ranging from turbogas power plants to wind turbines [1]. In particular, the performance of turbines and turbo-compressors are strongly influenced by transition. For instance, being able to accurately control the transition point may allow engineers to reduce losses in low-pressure turbines, thus producing more efficient engines. The same control may lead to the design of more compact axial compressors, using highly loaded blade rows. Moreover, transition has a remarkable impact on the heat-exchange process, therefore, the control of the transition point becomes fundamental to design effective cooling systems for high-temperature blade rows, which in turn represent the core of high efficiency power plants. A thorough knowledge of the boundary layer transition mechanisms is essential to develop techniques to model [2,3] and control [4] it, in order to improve the performance of modern turbomachinery. It is a very challenging task, since

\* Corresponding author. Tel.: +39 0805963226; fax: +39 0805963411  
E-mail address: [depalma@poliba.it](mailto:depalma@poliba.it)

transition is a highly non-linear phenomenon, which involves a wide range of scales and depends on many variables such as pressure gradient, free-stream turbulence intensity, fluid properties, body surface roughness, etc. One of the most peculiar aspects of shear flows is that they may experience a sudden transition from an ordered motion to a complex turbulent dynamics in response to finite amplitude disturbances. In boundary-layer flows, such a phenomenon is known as bypass transition in contrast with the natural transition mechanism based on the slower amplification of Tollmienn-Schlichting waves. Bypass transition is very common in turbomachinery flows since it originates from the high level of the freestream turbulence, which is typical of such internal flows. In the present work, a numerical study of the influence of the freestream turbulence on bypass transition in a boundary-layer flow over a flat plate is provided.

Several scenarios have been proposed in the last decade to describe such a fast route of transition [5,6]. The more established one is grounded on the generation of low-amplitude ( $O(1/Re)$ ,  $Re$  being the Reynolds number) streamwise rolls which induce, by means of the *lift-up* effect,  $O(1)$  streaks eventually undergoing secondary instability of sinuous type [6,7]. Such streamwise-invariant flow structures have been found to provide at a given time the largest energy growth through linear non-normal mechanisms, thus representing the *linear optimal* disturbances for a boundary-layer flow. As proved by Luchini[8], when a shear flow is perturbed by an external source, disturbances of any shape tend to the optimal one, even when the initial perturbation is relatively far from the optimal [8]. In the past years, several authors have observed this types of structures in boundary-layer flows excited by free-stream turbulence (FST) of moderate intensity ( $Tu$ ) and integral length scale [5,7] ( $L$ ). However, recent observations in the presence of large amplitude localized turbulent slabs [9] or FST [10] of large  $Tu$  and  $L$  indicate the existence of a different path to transition, characterized by spanwise vortex structures in the early stages. In this high-energy FST scenario, streaks appear before breakdown, but they would not have a fundamental role in the transition process, which is characterized by localized finite-amplitude vortical structures.

In the last two years, a new optimization approach has been developed for determining the most "dangerous" perturbations in shear flows, based on the formulation of a fully-non-linear optimal growth problem. This approach has been applied recently to pipe [11], Couette [12,13] and boundary-layer flows [14–16], discovering the relevance of *non-linear* optimal perturbations which have a very different localized structure with respect to the linear ones and outgrow them, leading to transition through a very fast non-linear route (which will be hereafter called *optimal trajectory*). Nevertheless, no evidence has still been provided about the existence of such finite-amplitude structures in the process of transition arising by receptivity from environmental disturbances, such as free-stream turbulence, roughness at the wall, or acoustic waves.

In this work, an overall picture of the bypass transition scenarios is provided in order to determine whether, and under which conditions, the transitional flow structures are correlated with the linear or non-linear perturbations on the optimal trajectory. To this end, the NS equations for an incompressible fluid are solved by direct numerical simulation (DNS) and the first phases of formation of turbulent spots are studied. Finally, a law to predict the transition location is provided, depending on the freestream turbulence intensity and its integral length scale.

## 2. Problem formulation

Bypass transition is induced by synthetic turbulence introduced at the inlet of the computational domain, obtained as a superposition of the continuous modes of the Orr–Sommerfeld and Squire operators [5,7]. We select 400 eigenmodes, each one associated with a three-dimensional wave-vector,  $\mathbf{k} = (\alpha, \gamma, \beta)$ , where  $\alpha, \gamma, \beta$  are the wavenumbers in the streamwise, wall-normal, and spanwise direction. Since turbulence is introduced at the inlet of the computational domain, the streamwise wavenumber is replaced by the temporal frequency  $\omega$  using the relation  $\omega = \alpha U_\infty$ ,  $U_\infty$  being the free-stream velocity. For the turbulence to be isotropic and homogeneous, the Von Karman energy spectrum has been chosen. Following the formulation of Ref. [7], we introduce the *integral length scale*  $L = 1.8/k_{max}$  (where  $k_{max}$  is the magnitude of the wave-vector corresponding to the maximum energy eigenvector), and derive the following expression for the spectrum:

$$E(k) = \frac{2}{3} \frac{a(kL)^4}{(b + (kL)^2)^{17/6}} LTu^2 \quad (1)$$

with  $a = 1.606$  and  $b = 1.350$ . The integral length scale  $L$  indicates the main longitudinal scale of the turbulence, and is linked to the longitudinal two-point correlation length scale,  $L_{11} \approx 0.643L$  [17]. The eigenvectors associated with the

selected wavenumbers are computed solving the Orr–Sommerfeld and Squire problem, and summed up to obtain the inlet synthetic turbulence, having integral length scale  $L$  and intensity  $Tu = \sqrt{(u_{rms}^2 + v_{rms}^2 + w_{rms}^2)}/3$  ( $u_{rms}, v_{rms}, w_{rms}$  being the root mean square values of the streamwise, wall-normal, and spanwise components of velocity). At inlet points, the turbulent fluctuations are superposed to the Blasius velocity profile, providing the boundary condition for solving the governing Navier-Stokes equations for an incompressible fluid:

$$\begin{aligned} \frac{\partial \mathbf{u}}{\partial t} + (\mathbf{u} \cdot \nabla) \mathbf{u} &= -\nabla p + \frac{1}{Re} \nabla^2 \mathbf{u}, \\ \nabla \cdot \mathbf{u} &= 0. \end{aligned} \quad (2)$$

The Reynolds number is defined as  $Re = U_\infty \delta_0^* / \nu$ ,  $\nu$  being the kinematic viscosity,  $\delta_0^*$  the inflow boundary-layer displacement thickness,  $p$  the pressure, and  $\mathbf{u} = (u, v, w)$ , where  $u, v, w$  are the streamwise, wall-normal, and spanwise velocity components. All of the simulations are performed at  $Re = 300$ . For  $Tu \geq 4.5\%$ , a reference domain with  $L_x = 500$ ,  $L_y = 70$  and  $L_z = 90$  is chosen,  $x, y$ , and  $z$  being the streamwise, the wall-normal, and the spanwise directions, respectively; whereas, for  $Tu < 4.5\%$  the domain (as well as the grid points) have been doubled in the streamwise direction. The dependence of the results with respect to the domain lengths  $L_x, L_y$ , and  $L_z$ , has been checked. The inlet of the computational domain is located at  $x_{in} = 100$ . Based on a grid-convergence analysis, a mesh made by  $551 \times 200 \times 181$  points – stretched in the wall-normal direction – has been selected for the reference domain. The grid sizes at the wall in plus units have been found consistent with the ones in Ref. [10]. The NS equations are integrated by a second-order-accurate fractional step method [18]. The following boundary conditions are applied: a convective condition at outlet points; the no-slip boundary condition at the bottom wall; zero perturbation with respect to the Blasius flow at the upper-boundary; periodicity for the three velocity components in the spanwise direction. The results have been validated by reproducing the decay of  $Tu$  and the skin-friction coefficient ( $C_f$ ) space distribution obtained in Ref. [7] for  $L = 5$  and  $Tu = 4.7\%$ , and Ref. [10] for  $L = 35$  and  $Tu = 6.7\%$ .

### 3. Results

We performed 28 simulations for  $Tu = 3.5\%, 4.5\%, 5.5\%, 6.5\%$  and  $L = 5, 10, 15, 20, 25, 30, 35$ . The smallest values of  $Tu$  are larger than the typical threshold for bypass transition (i.e.,  $Tu > 1\%$ ), so 'natural' transition via Tollmien-Schlichting waves is not observed. The largest values of  $Tu$  and  $L$  are typical of many practical applications involving high-speed flows in complex geometries such as turbomachinery [1,3] and combustors. Figure 1 shows the streamwise velocity and vorticity fluctuations (surfaces for  $u' = -0.2$  and  $\omega_x' = \pm 0.1$ ) extracted at  $t = 2250$  from a DNS with  $L = 35$  and two values of  $Tu$  ( $Tu = 3.5\%, 6.5\%$  from top to bottom). For  $Tu = 3.5\%$  (first frame), the receptivity region is characterized by mildly oscillating streamwise streaks which undergo secondary instability and breakdown. One can also notice that strong vortical structures appear only at a large abscissa, where strong sinuous oscillation of the streaks are observed, leading to transition in a spanwise-localized flow region. For larger turbulence intensity, stronger oscillations of the streaks and more high-vorticity regions are observed already at smaller abscissae. Increasing further the turbulent intensity (second frame of Figure 1) leads to a much larger density of vortical structures and a higher localization of the low-momentum zones. A similar behaviour is observed when increasing the turbulence intensity for  $L = 5$  to  $L = 35$  for a given value of  $Tu$ . Thus, it appears that, for increasing  $Tu$  and  $L$ , the transition mechanism changes from the classical secondary instability of the streaks to a different scenario based on the occurrence of localized vortical structures. Recalling that the coherent structures recovered in the early phases of the former scenario are very well correlated to the structures found by a linear energy optimization [6,8], we conjecture that the latter scenario could be linked to the onset of localized finite-amplitude coherent structures, which might be well correlated to the ones on the non-linear optimal trajectory recently recovered in Ref. [14].

To verify such a conjecture, we compute non-linear optimal perturbations at  $Re = 300$  using the method employed in Ref. [14]. Since in Ref. [16] it has been shown that the structure of the non-linear optimal perturbation is only slightly dependent on the domain size and target time, we choose for the optimization a smaller domain with dimensions  $l_x = 200$ ,  $l_y = 20$ ,  $l_z = 10$ , and target time equal to 125. Concerning the initial perturbation energy,  $E_0$ , we bisect its value of  $E_0$  until we obtain the initial optimal perturbation of minimal energy capable of inducing transition. Thus, we are looking for localized flow structures, induced by receptivity to free-stream turbulence, which are similar to the flow structures found during the route to transition of such optimal perturbation (the "optimal" route). Such

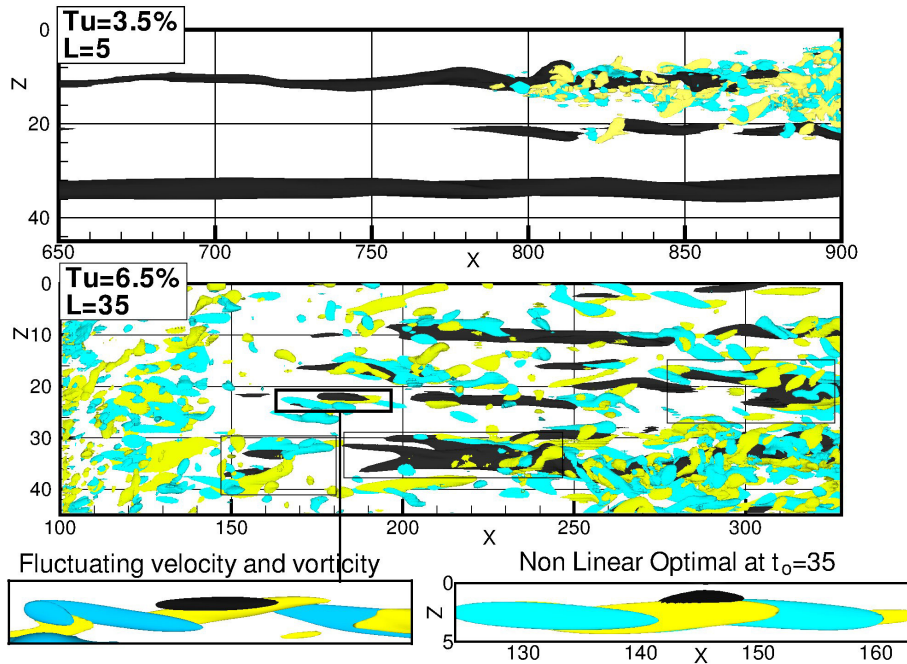


Fig. 1. Fluctuations of the streamwise component of the velocity (black surfaces for  $u' = -0.2$ ) and vorticity (yellow and blue for  $\omega'_x = \pm 0.1$ ) extracted at  $t = 2230$  from the DNS with  $Tu = 3.5\%$ ,  $L = 5$  (top) and with  $Tu = 6.5\%$ ,  $L = 35$  (middle), for  $0 < y < 10$ . Bottom left: zoom of the region boxed by the thick line. Bottom right: non-linear optimal disturbance at  $t_o = 35$  ( $\hat{\omega}_x = \pm 0.1$ ,  $\hat{u} = -0.1$ )

structures should outgrow the others during the evolution towards transition. In order to avoid any confusion with the DNS time,  $t$ , we define  $t_o$  as the evolution time during the "optimal" route with respect to the initial time of the optimization.

The bottom right frame of Figure 1 shows the perturbation extracted at  $t_o = 35$  from the non-linear optimal route to transition (half of the domain is shown in  $z$ ). It is composed by streamwise-inclined vortices ( $\hat{\omega}_x$  being the streamwise vorticity perturbation) along a region of high negative streamwise perturbation  $\hat{u}$ . Similar structures are indeed observed in the DNS for high values of  $Tu$  and  $L$ , the bottom left frame of the Figure showing one of them extracted from the DNS. Structures recalling the ones on the non-linear optimal trajectory are often recovered within the flow at high  $Tu$  and  $L$ : the large streamwise fluctuations often show a  $\Lambda$ -shape (see the bottom left inset of Figure 2), and in the receptivity zone the vortices are often recovered in an alternated inclined fashion (see the boxed regions in the middle frame of Figure 1). It is worth pointing out that vortical structures are observed also at lower values of  $Tu$  and  $L$ , but they are placed on the flanks of well-developed streamwise streaks (see the first frame of figure 1). Such streaks are still not formed in the receptivity region for higher values of  $Tu$  and  $L$  (second frame of figure 1). In fact, in the latter case, the vortices do not appear to be generated by a secondary instability of the streaks, but rather by the onset of localized structures strongly recalling the ones on the non-linear optimal trajectory. Thus, it can be argued that, among all of the localized flow structures, some "quasi-optimal seeds" can be found which would outgrow the other structures and lead to transition following a route close to the evolution of the non-linear optimal perturbation.

This can be confirmed by computing the correlation between the structures recovered within the boundary layer ( $\mathbf{u}'_{DNS}(t)$ ) and the perturbations on the non-linear optimal trajectory ( $\hat{\mathbf{u}}_{OPT}(t_o)$ ) at various times. We define a correlation,

$$C(t, t_o) = \max_{x,z} \left[ \frac{\langle \mathbf{u}'_{DNS}, \hat{\mathbf{u}}_{OPT} \rangle}{\sqrt{\langle \mathbf{u}'_{DNS}, \mathbf{u}'_{DNS} \rangle} \sqrt{\langle \hat{\mathbf{u}}_{OPT}, \hat{\mathbf{u}}_{OPT} \rangle}} \right] \quad (3)$$

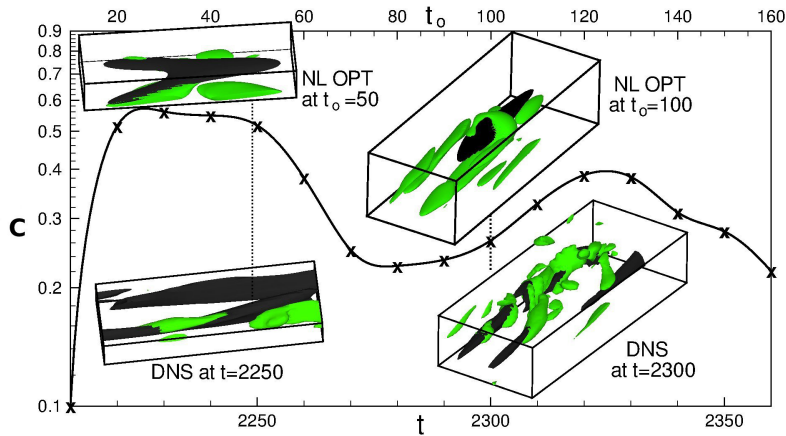


Fig. 2. Time evolution of the correlation  $C(t, t_o)$ . The top insets show the non-linear optimal perturbation at  $t_o = 50$  and  $t_o = 100$ ; the bottom insets show the structures extracted from the DNS with  $Tu = 6.5\%$ ,  $L = 35$  at  $t = 2250$  and  $t = 2300$ : green surfaces represent vortical structures (Q-criterion); black surfaces represent streamwise velocity fluctuations (bottom) and perturbations (top) with values  $-0.15$  (left) and  $-0.2$  (right).

where the symbol  $\langle \rangle$  indicates the energy inner product. For computing the correlation, the perturbations on the optimal trajectory are enclosed in a box of dimensions:  $\Delta z = l_z/2$ , to relax the symmetry with respect to the  $z = 0$  plane;  $\Delta y = l_y$ ;  $\Delta x$  equal to the length of the region in which the perturbation on the optimal trajectory is greater than 1% (therefore, the resulting length varies with  $t_o$ ). The enclosing box is displaced over the DNS velocity field in both  $x$  and  $z$  throughout the whole receptivity zone, i.e., from the inlet of the computational domain up to the abscissa at which the skin friction coefficient  $C_f$  overtakes its minimum value by 10%. Figure 2 shows an example of the time evolution of the correlation for the region zoomed in figure 1, which have been moved in time in the streamwise direction following the optimal disturbance evolution. Notice that, in this particular case, the DNS time,  $t$ , and the optimization time,  $t_o$ , are shifted by an interval of 2200 units. The correlation reaches values greater than 0.5 for about 40 time units, corresponding to the early development of the inclined and  $\Lambda$  vortices (compare the insets on the left in figure 2). Such a value decreases and then rises again at a time which corresponds to the formation of the hairpin vortices (compare the insets on the right in figure 2). Notice that, as it could be anticipated, for  $t_o < 20$  the correlation show very low values, since quasi-optimal perturbations have still not been created by the receptivity process. In fact, one has to consider that the initial optimal perturbations ( $t_o = 0$ ) is composed by upstream-inclined vortical structures [16], which are not likely to be induced by the freestream turbulence.

In order to generalize the results, the correlation  $C$  has been computed for several DNS snapshots in a time window  $2000 < t < 2200$ , and the resulting values are averaged (the  $t$ -averaged value is indicated by  $\bar{C}$ ). Considering both space and time shifts, up to 450000 values of correlations have been computed for each value of  $Tu$  and  $L$ . Moreover, in order to account for the time evolution of the structures on the optimal trajectory, the correlation values have been calculated for perturbations taken at several optimization times ( $t_o$ ), ranging from 10 to 150. It is worth noticing that the correlation used here is much more restrictive than the one used in the literature for recovering exact coherent structures in small periodic domains [19], since the correlating velocity vectors are not rescaled in amplitude with respect to the mean velocity, as done by Tutty & Kerswell (2007), for instance. This means that correlation values close to 1 can be reached for a DNS velocity field almost coincident in both amplitude and shape to the one on the optimal trajectory, which is very unlikely since here transition is reached in a natural way by a receptivity mechanism. In order to establish which range of values is indicative of a good match, we have computed the correlation parameter for perturbations on the *linear* optimal trajectory (obtained by a linear optimization and then rescaled in energy to reach the laminar-turbulent boundary), essentially composed by streamwise streaks which have been found to populate the receptivity zone for moderate values of  $Tu$ . Based on such computations, it appears that time-averaged correlation values larger than 0.5 are very rarely detected in the flow, for both linear and non-linear perturbations. It is worth pointing out that instantaneous correlation values up to 0.75 can be found for perturbations on the linear and

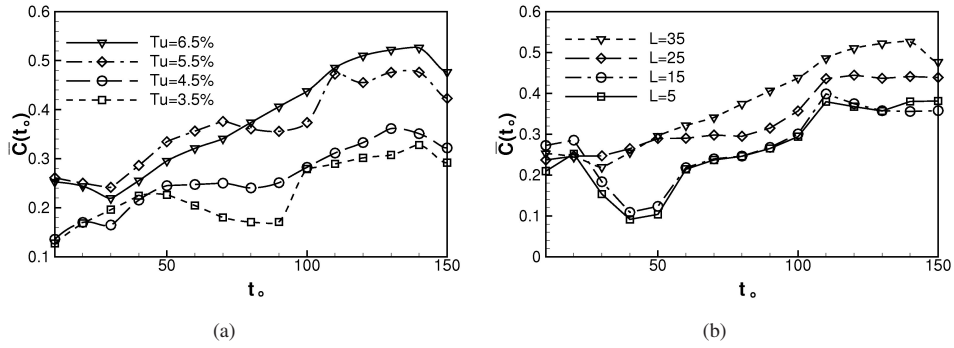


Fig. 3. Values of the time-averaged correlation  $\overline{C}(t_o)$  versus the optimization time, computed between the perturbations on the non-linear optimal trajectory at several times  $t_o$  and the DNS velocity field obtained for: (a)  $L = 35$  and  $Tu = 3.5\%, 4.5\%, 5.5\%, 6.5\%$ ; (b)  $Tu = 6.5\%$  and  $L = 5, 15, 25, 35$ .

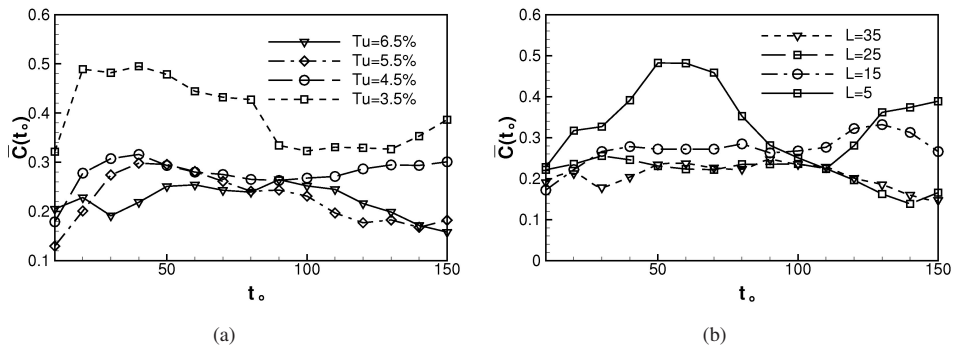


Fig. 4. Values of the time-averaged correlation  $\overline{C}(t_o)$  versus the optimization time, computed between the perturbations on the linear optimal trajectory at several times  $t_o$  and the DNS velocity field obtained for: (a)  $L = 35$  and  $Tu = 3.5\%, 4.5\%, 5.5\%, 6.5\%$ ; (b)  $Tu = 6.5\%$  and  $L = 5, 15, 25, 35$ .

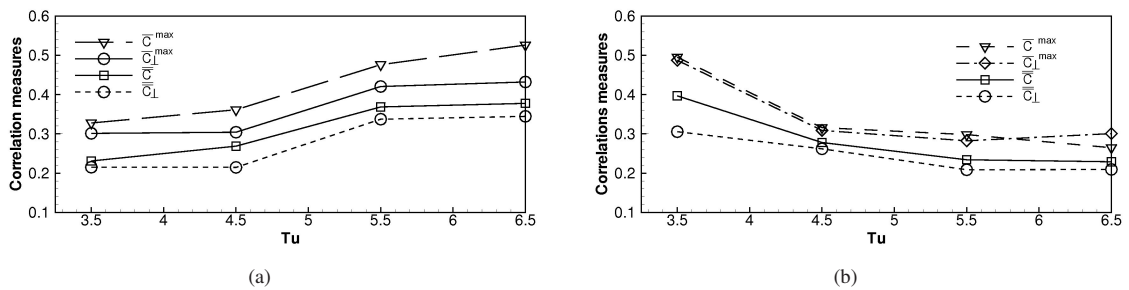


Fig. 5. Maximum and  $t_o$ -averaged values of the total ( $\overline{C}^{max}$ ,  $\overline{C}$ ) and of the cross-stream correlation ( $\overline{C}_\perp^{max}$ ,  $\overline{C}_\perp$ ), computed between the DNS velocity field obtained for  $L = 35$  and  $Tu = 3.5\%, 4.5\%, 5.5\%, 6.5\%$ , and the perturbations on the (a) non-linear, and (b) linear optimal trajectory.

non-linear optimal trajectory. However, we consider that such instantaneous correlation measures are not relevant to the present analysis, since we would like to provide a measure of the likelihood of the occurrence of certain structures in the considered flow, and not the maximum correlation value which can be found under certain particular conditions.

Figure 3 (a) shows the correlation values between the perturbations on the non-linear optimal trajectory at several times  $t_o$ , and the DNS velocity field obtained for  $L = 35$  and the four  $Tu$  values considered here. It appears that the correlation is rather low at small optimization times, and then grows with time until  $t_o \approx 130$ , which is close to the target time of the non-linear optimization, approximately corresponding to the time of formation of the hairpin vortex. This result could be anticipated, considering that for very low optimization times, the initial optimal perturbation is composed by upstream-inclined vortical structures [16], which are not likely to be induced by free-stream turbulence, whereas  $\Lambda$  and hairpin structures appear to be naturally generated by a receptivity process. Moreover, the correlation curves are found to raise for increasing values of  $Tu$ . Correlation values of the order of 0.5 are reached for  $Tu = 5.5\%$ ,  $6.5\%$ , confirming that structures similar to the non-linear optimal ones are recovered for sufficiently high values of  $Tu$ . A similar trend is observed for the correlation value versus  $L$ , as shown in Figure 3 (b) for  $Tu = 6.5\%$  and four values of  $L$ . For comparison purposes, Figure 4 shows the corresponding correlation values obtained between the perturbations on the linear optimal trajectory and the DNS snapshots extracted for the same values of  $Tu$  and  $L$ . Again, the maximum correlation values are of the order of 0.5, but now the largest values are observed for the lowest values of  $Tu$  and  $L$ . One can also observe that in this case the correlation curves peak at lower times, indicating that the largest similarities are recovered for perturbations which have not yet been influenced by non-linear effects. This could be anticipated, considering that for the lowest values of  $Tu$  and  $L$  considered here, we know that quasi-linear streaks are found to populate a very long region of the flow, until secondary instability sets in (see the first frame of Figure 1). Therefore, this result can be considered as a validation of the proposed correlation approach. The results for the linear and non-linear cases are summarized in figure 5 (a) and (b), respectively, providing, for the values of  $Tu$  and  $L$  considered before, the maximum value of the correlation  $\bar{C}^{max}$ , and its averaged value with respect to  $t_o$ ,  $\bar{C}$  (notice that such a  $t_o$ -averaging is different from the  $t$ -average mentioned before). Moreover, to validate the results, a different measure of the correlation is also considered, namely, the cross-stream correlation  $C_{\perp}$ , which is defined following equation (3) using the cross-stream velocity vector, i.e.,  $\mathbf{u}^{\perp} = (v, w)$  [19], for both DNS and optimal velocity fields. Such a correlation accounts for the fact that, in shear flows, the  $u$  component dominates the flow field and the correlation value [19], and for this reason it is more restrictive than the first one. The first frame of Figure 5 shows that, when perturbations on the non-linear optimal trajectory are considered, all of the considered correlation measures (maximum and  $t_o$ -averaged total and cross-stream correlation) are found to increase with the turbulence intensity, for a given  $L$ . On the other hand, when perturbations on the linear optimal trajectory are considered, the correlations values decrease with  $Tu$ . These results indicate that, when the flow is excited with turbulence of large intensity and length scale (namely,  $Tu > 4.5\%$  and  $L > 20$ ), the coherent structures in the transitional region are likely to show some features of the disturbances on the non-linear optimal trajectory. On the other hand, when the free-stream turbulence is not large enough (or it decays too rapidly) the transitional region is mostly characterized by the most energetic structures with low amplitude [8], namely, the disturbances on the linear optimal trajectory, inducing the formation of elongated streaks which undergo secondary instability.

These two scenarios appear to reflect the features of two plausible relative attractors on the laminar-turbulent boundary recently identified for the boundary-layer flow starting from a linear and non-linear optimal disturbance [20] (see also [21,22]).

We have thus outlined two routes to transition, which are triggered at different values of  $Tu$  and  $L$ . To distinguish between the two scenarios, we introduce a simple parameter defined as follows. Since the main difference between the flow structures is in the longitudinal correlation of the  $u'$  fluctuation (namely, the presence of localized patches of  $u'$  instead of elongated streaks), we use the following streamwise average parameter:

$$\mathcal{U} = \max_{y,z} \frac{\int_{x_{in}}^{x_T} u'(x, y, z) dx}{x_T - x_{in}} \quad (4)$$

where  $x_T$  is the transition-onset abscissa, i.e., the  $x$  value at which the  $C_f$  overtakes its minimum by a percentage  $p$  (with  $p = 1\%$ ,  $10\%$ ,  $20\%$ , the results do not show remarkable differences). Figure 6 provides the contours of  $\mathcal{U}$  in the  $L - Tu$  plane, plotted for  $p = 1\%$ : for low values of  $Tu$  and  $L$ ,  $\mathcal{U}$  is rather high, and decreases for increasing values of such parameters. For high  $Tu$  and  $L$ , the amplitude of  $u'$  is large, but the fluctuations are poorly correlated in  $x$ , resulting in small values of  $\mathcal{U}$ ; on the other hand, for low  $Tu$  and  $L$ , the amplitude of  $u'$  is lower, but the fluctuations are strongly correlated in  $x$ , resulting in large values of  $\mathcal{U}$ . Relating the values of  $\mathcal{U}$  with the structures observed within the flow, we can identify three regions in the  $L - Tu$  plane: i) for  $\mathcal{U} > 0.23$ , the transition scenario is the *linear*

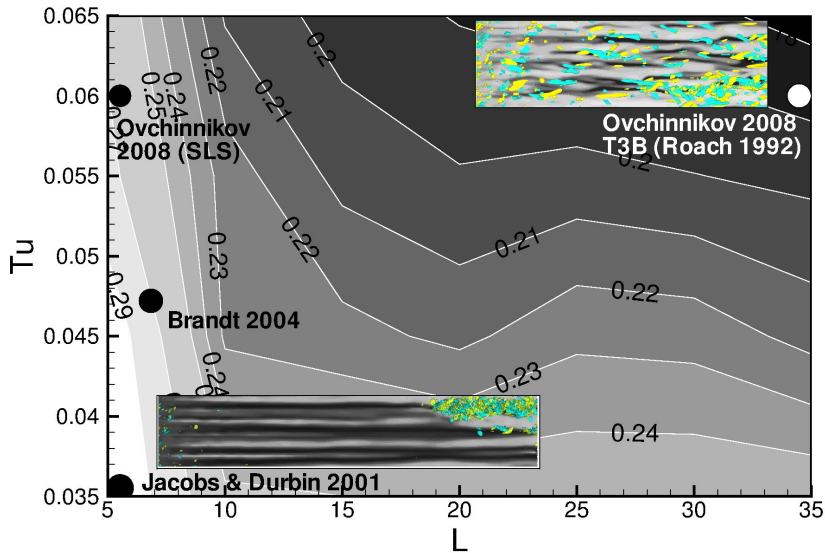


Fig. 6. Contours of the  $\mathcal{U}$  parameter in the  $L - Tu$  plane. The two insets show the typical structures of the two transition scenarios. For the *linear* scenario (bottom): streamwise streaks (black and white contours on the plane  $y = 1$ ) with vortices on their flanks (yellow and blue surfaces for  $\omega'_x = \pm 0.1$ ). For the *non-linear* scenario (top): localized velocity fluctuations with large-amplitude vortical zones, often in the form of  $\Lambda$  or hairpin structures (the values of  $u'$  and  $\omega'_x$  are the same as in the bottom inset). The dots indicate the  $L - Tu$  values of some DNS results available in the literature.

one (i.e., the one based on the perturbations on the linear optimal trajectory, the streaks); ii) for  $0.23 > \mathcal{U} > 0.2$ , both scenarios are observed; iii) for  $\mathcal{U} < 0.2$ , the scenario is the *non-linear* one (i.e., the one based on the disturbances on the non-linear optimal trajectory). It is worth to notice that the threshold value of  $\mathcal{U}$  for which we observe the *linear* scenario (0.23) is very close to the critical amplitude of the streaks at which secondary instability is triggered [6]. Moreover, our observations appear to be in agreement with the results available in the literature, some of which are indicated by dots in figure 6. For instance, elongated streaks undergoing breakdown are observed in [5] and [7], with values of  $Tu$  and  $L$  typical of the *linear* scenario. On the other hand, in [10] two simulations are performed, one in the *linear*, the other in the *non-linear* zone; in the latter, the authors observe that transition is due to the creation of spanwise vortices rather than streamwise streaks.

Concerning the *linear* scenario, the linear optimal-growth theory [8,23] shows that disturbances grow as  $Re_x^{1/2}$  (with  $Re_x = xU_\infty/\nu$ ). Andersson et al. [23] proposed that transition is triggered when the root mean square of the streamwise velocity fluctuation  $u_{rms} \approx Re_x^{1/2} Tu$  achieves a critical value [8]. Such a model is found to apply well for cases with low  $Tu$  and  $L$  (see the experimental data in [24,25]), but, being based on the linear optimal growth theory, it does not take into account the growth of the other components of the velocity, which are not negligible in the *non-linear* scenario. More recently, Brandt et al. [7] proposed a different law,  $u_{rms} \approx Re_x^{1/2} Tu^2$ , linked to a two-step receptivity process, in which the streamwise vorticity penetrates the boundary layer due to nonlinear interactions and then induces the formation of streaks due to the linear lift-up effect. In order to establish which of these laws is valid in the cases considered here, we analyze the variation in the streamwise direction of the variable  $\tilde{u}_{rms} = \sqrt{(u_{rms}^2 + v_{rms}^2 + w_{rms}^2)}$ . Figure 7 provides the spatial distribution of the wall-normal maximum of  $\tilde{u}_{rms}$ , computed in six DNSs with different values of  $Tu$  and  $L$ . The small vertical lines indicate, for each computation, the value  $Re_x^{1/2}$  at the transition location ( $Re_{x^*}^{1/2}$ ) measured at the abscissa where  $C_f$  reaches its minimum value [10]. One can observe that transition is always triggered when  $\tilde{u}_{rms}^{max}$  reaches an estimated value of 0.18 (within a confidence interval indicated by the gray zone). We have verified that, for  $Tu = 3.5\%$ ,  $u_{rms}^{max} \approx \tilde{u}_{rms}^{max}$  at the transition abscissa, confirming the experimental findings in [24,25]; however, for  $Tu = 6.5\%$ ,  $u_{rms}^{max}$  is much lower than  $\tilde{u}_{rms}^{max}$  at the transition location. In all of the cases, the variable  $\tilde{u}_{rms}^{max}$  varies almost linearly with  $Tu$ , indicating that if all of the velocity components are considered, the law for transition prediction can be the same for all of the values of  $Tu$  and  $L$ . Moreover, transition occurs at a

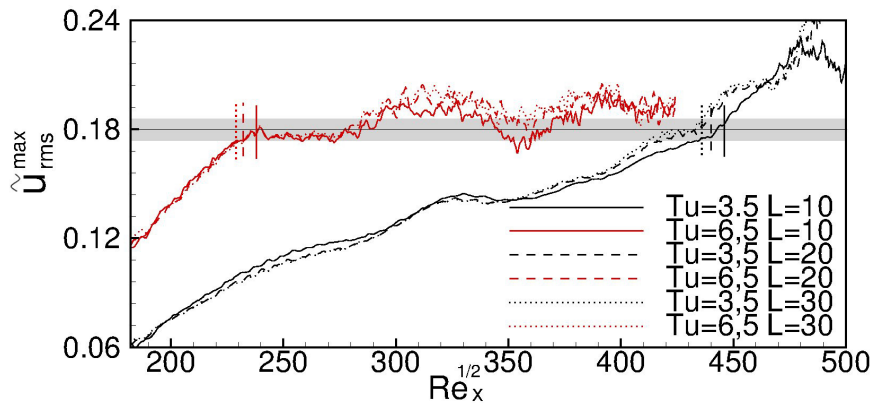


Fig. 7. Wall-normal maximum of  $\tilde{u}_{rms} = \sqrt{(u_{rms}^2 + v_{rms}^2 + w_{rms}^2)}$  for six DNSs with different values of  $Tu$  and  $L$ . The small vertical lines indicate the values of  $\sqrt{(Re_{x_T})}$  measured at the abscissa where  $C_f$  reaches its minimum. In all cases, transition is triggered when  $\tilde{u}_{rms} \approx 0.18$  (the gray zone indicates the confidence interval).

lower abscissa for increasing values of  $L$ , indicating that the integral length scale should be taken into account in a law predicting the transition location. Thus, we tried to match our numerical data with both of the above laws for transition prediction, obtaining good results using the one proposed by Andersson et al. [23]. Furthermore, several functions of  $L$  have been employed to improve such a law, taking into account the dependence on the integral length scale. Finally, the following modified law for transition prediction, valid for both transition scenarios, has been obtained:

$$Re_{x_T}^{1/2} Tu \frac{L}{L+1} = const. \quad (5)$$

Measuring the values of the transition abscissae in the 28 DNSs performed here, we found that the right hand side of the equation is equal to  $14.5 \pm 0.4$ , very close to the equivalent value obtained by Fransson et al. [25] using a method based on intermittency, namely  $\sqrt{196}$ , considered here.

#### 4. Concluding remarks

The results provided in this paper indicate the possibility that, in a flat-plate boundary layer excited by free-stream turbulence (FST) with large intensity ( $Tu > 4.5\%$ ) and integral length scale ( $L > 20$ ) transition from laminar to turbulent flow follows a purely non-linear route correlated to the evolution of non-linear optimal perturbations. Our results are in agreement with the conclusions of the work in Ref. [10] in which the effect of the FST length scale on the transition mechanism at high-amplitude FST is studied. In fact, we find that, for such high values of FST intensity and length scale, transition is initiated by localized perturbations directly induced inside the boundary layer by receptivity to free-stream turbulence. This scenario is different from that observed at lower values of FST intensity and length scale [7] since in the latter case transition is initiated by the formation of streaks which experience secondary instability producing localized vortical structures. An important difference with respect to the analysis in Ref. [10] is that we do not take into account the leading edge of the flat plate, so that the localized vortical structures we observe are generated only by the action of the FST. Moreover, we provide a detailed analysis to put in evidence that those flow structures are well correlated with structures on the non-linear optimal trajectory towards turbulence. We provide also a criterion to distinguish these two transition scenarios by employing a simple parameter linked to the streamwise localisation of high- and low-momentum zones. Finally, we propose a simple law for the prediction of the transition onset abscissa, based on both turbulence intensity and integral length scale, which is valid for both transition scenarios. Such results highlight the importance of non-linear coherent structures in boundary-layer transition and motivate further research about non-linear optimal disturbances with the aim of better understanding the different paths to transition.

Some computations have been performed on the Power 6 of the IDRIS, France.

## References

- [1] Mayle, R.. The role of laminar-turbulent transition in gas turbine engines . ASME J Turbomach 1991;113:509–537.
- [2] Cutrone, L., De Palma, P., Pascasio, G., Napolitano, M.. An evaluation of bypass transition models for turbomachinery flows. Int J Heat Fluid Flow 2007;655:161–177.
- [3] Cutrone, L., De Palma, P., Pascasio, G., Napolitano, M.. Predicting transition in two- and three-dimensional separated flows . International Journal of Heat and Fluid Flow 2008;29:504–526.
- [4] Bewley, T.R., Moin, P., Temam, R.. Dns-based predictive control of turbulence: an optimal benchmark for feedback algorithms flows. J Fluid Mech 2001;447:179–225.
- [5] Jacobs, R.G., Durbin, P.A.. Simulations of bypass transition . J Fluid Mech 2001;428:185–212.
- [6] Andersson, P., Brandt, L., Bottaro, A., Henningson, D.S.. On the breakdown of boundary layer streaks . J Fluid Mech 2001;428:29–60.
- [7] Brandt, L., Schlatter, P., Henningson, D.S.. Transition in a boundary layers subject to free-stream turbulence . J Fluid Mech 2004;517:167–198.
- [8] Luchini, P.. Reynolds number independent instability of the Blasius boundary layer over a flat surface: optimal perturbations . J Fluid Mech 2000;404:289–309.
- [9] Wu, X., Moin, P.. Direct numerical simulation of turbulence in a nominally-zero-pressure-gradient flat-plate boundary layer . J Fluid Mech 2009;630:5–41.
- [10] Ovchinnikov, V., Choudhari, M.M., Piomelli, U.. Numerical simulations of boundary-layer bypass transition due to high-amplitude free-stream turbulence . J Fluid Mech 2008;613:135–169.
- [11] Pringle, C.C.T., Kerswell, R.. Using nonlinear transient growth to construct the minimal seed for shear flow turbulence . Phys Rev Lett 2010;105:154502.
- [12] Monokrousos, A., Bottaro, A., Brandt, L., Di Vita, A., Henningson, D.S.. Non-equilibrium thermodynamics and the optimal path to turbulence in shear flows . Phys Rev Lett 2011;106:134502.
- [13] Cherubini, S., De Palma, P.. Non-linear optimal perturbations in a Couette flow: bursting and transition . J Fluid Mech 2013;716:251–279.
- [14] Cherubini, S., De Palma, P., Robinet, J., Bottaro, A.. Rapid path to transition via non-linear localized optimal perturbations in a boundary-layer flow . Phys Rev E 2010;82:066302.
- [15] Cherubini, S., Robinet, J.C., Bottaro, A., De Palma, P.. Optimal wave packets in a boundary layer and initial phases of a turbulent spot . J Fluid Mech 2010;656:231–259.
- [16] Cherubini, S., De Palma, P., Robinet, J.C., Bottaro, A.. The minimal seed of turbulent transition in a boundary layer . J Fluid Mech 2011;689:221–253.
- [17] Tennekes, H., Lumley, J.L.. A first course in turbulence . MIT press 1972;.
- [18] Verzicco, R., Orlandi, P.. A finite-difference scheme for the three-dimensional incompressible flows in cylindrical coordinates . J Comp Phys 1996;123(2):402–414.
- [19] Kerswell, R., Tutty, R.O.. Recurrence of travelling waves in transitional pipe flows . J Fluid Mech 2007;584:69–101.
- [20] Cherubini, S., De Palma, P., Robinet, J.C., Bottaro, A.. Edge states in a boundary layer . Phys of Fluids 2011;23:051705.
- [21] Duguet, Y., Schlatter, P., Henningson D. S. Eckhardt, B.. Self-sustained localized structures in a boundary-layer flow . Phys Rev Lett 2012;108:044501.
- [22] Biau, D.. Laminar-turbulent separatrix in a boundary layer flow . Phys Fluids 2012;24:034107.
- [23] Andersson, P., Berggren, M., Henningson, D.S.. Optimal disturbances and bypass transition in boundary layers . Phys Fluids 1999;11(1):134–150.
- [24] Matsubara, M., Alfredsson, P.. Disturbance growth in boundary layers subjected to free-stream turbulence . J Fluid Mech 2001;430:149–168.
- [25] Fransson, J., Matsubara, M., Alfredsson, P.H.. Transition induced by free stream turbulence . J Fluid Mech 2005;527(10):1–25.